Wu and Pyo *Int J Concr Struct Mater* (2025) 19:13
https://doi.org/10.1186/s40069-024-00747-z

International Journal of Concrete Structures and Materials

RESEARCH

Open Access

Effects of Vibration-Reducible Cementitious Materials on the Acoustic and Structural Responses of Buildings Adjacent to Urban Railway Systems: A Numerical Approach

Siyu Wu[1,2] and Sukhoon Pyo[2*]

Abstract

Some studies have developed different kinds of vibration-reducible construction materials. However, no existing study has applied these materials in a building to prove their effectiveness at a structural level. Besides, much of the related research has focused only on measuring sound pressure or vibration levels within buildings adjacent to railway systems. Although some studies have provided methods to predict the vibration of a building structure, they cannot determine the train-induced sound pressure level simultaneously. Therefore, this study used the finite element model to simulate an existing building structure to prove the effectiveness of this method. Based on the combination of the acoustic and solid interaction modules in the finite element analysis method, the vibration and sound levels of buildings based on different kinds of vibration-reducible cementitious materials were estimated using different models. The results show that vibration-reducible cementitious materials can reduce vibration velocity and sound pressure levels by up to 7.1 dB and 5.2 dB with an increased floor height, respectively. In addition, reduced vibration can decrease structure-borne noise by up to 2.9 dB. A further parametric study shows that cementitious materials with a relatively high elastic modulus, a high damping loss factor, and low density can be effective for vibration and sound reduction.

Keywords Vibration reducibility, Vibration velocity level, Displacement, Sound pressure, Structure-borne noise, Finite element model

1 Introduction

The simulation of train-induced vibration has been studied for the last three decades, with some researchers developing different methods to predict train-induced vibration, and most of the research focused on train-induced ground vibrations and vibration transmission in the soil (Amir Kaynia et al., 2000; Auersch, 2005; Connolly et al., 2013; Fu & Wu, 2019; Hunt, 1991, 1996; Kouroussis et al., 2014), omitting noise due to the passage of rolling stocks and the vibration transmission within buildings. However, with urban development, train-induced building vibration and structure-borne noise are deteriorating the urban living environment, especially buildings located near urban railway systems. However, existing numerical analysis methods for train-induced ground or soil vibration are insufficient for predicting the train-induced vibration and structure-borne noise within a building due to the vibration transmission in the building, and only a few numerical analysis methods

Journal information: ISSN 1976-0485 / eISSN 2234-1315.

*Correspondence:
Sukhoon Pyo
shpyo@unist.ac.kr
[1] Chongqing Technology and Business Institute, Chongqing Open University, Chongqing 400052, China
[2] Department of Civil, Urban, Earth, and Environmental Engineering, Ulsan National Institute of Science and Technology (UNIST), Ulsan 44919, Korea

were verified by the experimental data (Zou et al., 2020), most of which cannot analyze noise and vibration simultaneously. Moreover, this type of vibration and structure-borne noise exists in a low-frequency range (Ngai & Ng, 2000, 2003), which cannot be completely absorbed or reduced by noise barriers or resilient rail systems and which negatively affects people's health (Bolin et al., 2011; Maclachlan et al., 2018). Although some studies have developed vibration-reducible and noise-insulating cementitious materials (Wu & Pyo, 2023; Wu et al., 2022, 2023), there is a lack of efficient numerical analysis methods to predict the vibration and noise reduction behavior in the building structure based on the vibration- or noise-reducible materials.

Currently, the evaluation of building vibration and noise caused by the passage of trains is conducted by field experimental, empirical, and numerical methods. The experimental method is based on various field test data, as follows. The vibration response of the building surrounding the urban railway system can be recorded within the frequency domain or time domain, and these data can be transferred to estimate the building vibration level with transfer functions (Romero et al., 2012; With & Bodare, 2007; Zhu et al., 2023). This is a direct and accurate method, but it requires a significant number of field measurements to evaluate the vibration transmission characteristics of a building, so it will be time-consuming and costly, and it cannot evaluate structure-borne noise simultaneously. The empirical method is similar to the experimental method, also requiring field test data, but it can use empirical formulas to include more impact factors, such as train speed, wheel–rail contact force, and the distance between the railway system and buildings (Verbraken et al., 2011). Meanwhile, structure-borne noise can be estimated using empirical formulas based on the evaluated vibration response. However, these two methods can only apply to an existing building and cannot be applied to predict the vibration and structure-borne noise before a building is constructed. Meanwhile, the numerical analysis method offers a possible process by which the vibration response of a building structure before construction can be determine. Most numerical analysis methods are finite element methods (FEMs), and they cannot directly estimate the vibration response or sound pressure level within the building at the same time (Fiala et al., 2007; Kouroussis & Verlinden, 2013; Kouroussis et al., 2014; Lopes et al., 2014).

Based on the FEM, the acoustic–solid interaction coupling module is a kind of multiphysics method that enables the efficient and effective prediction of vibration and sound level at a structural level. Therefore, this new FE analysis method is appropriate for predicting train-induced vibration and sound. Compared with other methods, this multiphysics numerical analysis method can directly provide multiple results, such as the vibration velocity, displacement, and sound pressure level, without any post-calculation process after it completing model computation. In addition, it provides a possible method of predicting the vibration-reducibility and sound-insulating capacity of a building that might be constructed with vibration-reducible materials and that is located near urban railway systems. The prediction can help engineers devise better solutions to improve living conditions. Nevertheless, no existing study uses this efficient multiphysics numerical analysis method to predict the vibration and sound pressure within a building adjacent to the railway systems before construction.

Moreover, this multiphysics numerical method also provides a process for predicting vibration, sound pressure level, and structure-borne noise within a building structure based on the vibration-reducible cementitious materials. These developed materials showed high vibration reducibility under experimental conditions (Sharma et al., 2018; Wu & Pyo, 2023; Wu et al., 2023; Zheng et al., 2008), and previous studies indicate that increased vibration reducibility can decrease structure-borne noise (Chi et al., 2019; Li et al., 2015; Liang et al., 2021). Therefore, it is necessary to use this numerical analysis method to investigate the effect of vibration-reducible cementitious materials on the vibration and structure-borne noise reduction within a building structure.

In this study, an existing building structure was selected to verify whether the results from the FE analysis correspond to the previous study. After the FE analysis is proven valid, a simplified FE model with the acoustic–solid interaction module is used to predict the vibration and sound pressure level in a building that will be constructed with different types of vibration-reducible materials from previous studies and located near the railway system area. Meanwhile, the structure-borne noise level can be predicted, indirectly validating whether vibration-reducible materials can reduce structure-borne noise generation and transmission. Finally, relatively better vibration-reducible cementitious materials can be found, and a parametric study was conducted based on these materials to determine how the parameters of material properties affect vibration and sound reduction.

2 Materials and Test Methods

2.1 Materials

The materials used for the building structure were chosen from previous studies (Wu & Pyo, 2023; Wu et al., 2023); they have an average compressive strength above 30 MPa, and they have been proven vibration-reducible. The basic mechanical properties of these materials are shown in Table 1, and the mix proportions of each

Table 1 Physical parameters of vibration-reducible construction materials (Wu & Pyo, 2023; Wu et al., Jul. 2023)

Item	RF	Material 1	Material 2	Material 3	Material 4
Elastic modulus (E, GPa)	46.7	41.3	35.4	41.4	29.3
Poisson's ratio (μ)	0.25	0.27	0.20	0.26	0.21
Density (g/cm^3)	2.01	1.81	1.73	1.98	2.02
Damping loss factor (%)	1.66	1.70	1.78	1.83	1.95

material are shown in Table 2. According to previous studies, only concrete was considered in models for proofing the vibration-reducibility or noise insulation properties of construction materials (Chua et al., 1995; Hunt, 1996; Kouroussis et al., 2014), so reinforced concrete is not included in this study. Besides, this way can save time and computation resources.

2.2 Test Methods

2.2.1 Static Elastic Modulus Test

For simulation, the static elastic modulus of all materials is an important parameter. For each material, three cylinder specimens (Φ 10 cm × 20 cm) were cast and cured in room-temperature water for 27 d after demolding, and the static elastic modulus was tested at 28 d, according to ASTM C469 (ASTM, 2002), and was calculated using the following equation:

$$E = \frac{S_2 - S_1}{\varepsilon_2 - 0.000050} \tag{1}$$

where E is the elastic modulus, S_2 is the stress corresponding to 40% of the ultimate load, S_1 is the stress corresponding to a longitudinal strain of 50 millionths, and ε_2 is the longitudinal strain produced by stress S_2. The static elastic modulus test was conducted with three cylinder specimens, and the average value of the three testing results was used as the final elastic modulus for each mixture. The results for all materials are shown in Table 1.

2.2.2 Poisson's Ratio Test

Anson and Newman (Anson & Newman, 1966) and Ahmed (Ahmed, 2018) found that the static Poisson's ratio is similar to the dynamic Poisson's ratio, especially because the two values will be equal after 3 years. Therefore, this study used the dynamic Poisson's ratio as the actual Poisson's ratio of cementitious materials for a long-term building structure. The Poisson's ratio was measured following ASTM C215-19 (ASTM, 2019), where three 40 × 40 × 160 mm^3 prisms for each material are tested after 28 d of water curing. The setup of these two tests is shown in Fig. 1. For the dynamic Young's modulus measurement, a free–free is suspended by two ropes, an accelerometer is attached to one end surface, and a standard impact hammer applies force to another end surface in the longitudinal direction, as shown in Fig. 1a. Similarly, for the dynamic modulus of rigidity, the impact hammer force and acceleration are at the front side along the longitudinal direction, as shown in Fig. 1b. The Poisson's ratio is determined by the following equation:

$$\mu = \left(\frac{E}{2G}\right) - 1 \tag{2}$$

where E is the dynamic Young's modulus and G is the dynamic modulus of rigidity. E and G are measured by longitudinal and torsional impact resonance tests, respectively. E and G are calculated with Eqs. (3) and (4), respectively.

$$E = \frac{4LM(n_l)^2}{hw} \tag{3}$$

Table 2 Mix proportions for the construction materials used in this study (kg/m^3) (Wu & Pyo, 2023; Wu et al., 2022)

Mixture ID	Cement	Sand	HGM	GF	CS	Water	Compressive strength (MPa)			
RF	867	867				390.2	49.1			
Material 1		650.3	12.5				45.0			
Material 2		433.5			108.5		42.6			
Material 3		779		73.9			35.4			
–										
	Cement	Lime mud	Metakaolin	Silica fume	Fly ash	Water glass	Sand	Water	Superplasticizer	Compressive strength (MPa)
Material 4	628.6	125.7	100.6	50.3	10.6	55.8	1257.1	314.3	12.6	34.1

HGM hollow glass microsphere, *GF* graphite flakes, *CS* cenosphere

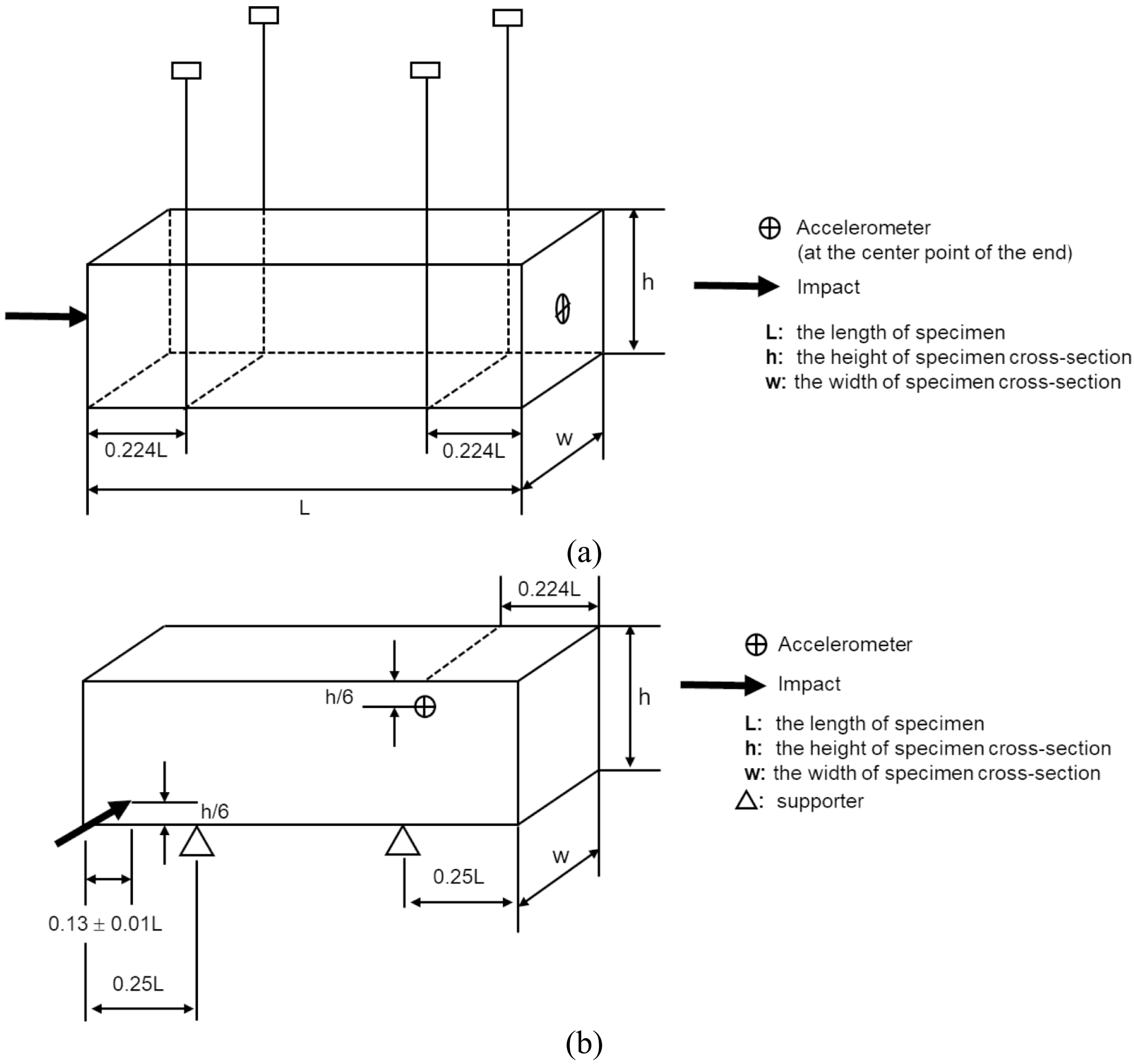

Fig. 1 **a** Setup of the longitudinal impact resonance test (Wu & Pyo, 2023), **b** the setup of the torsional impact resonance test

$$G = \frac{4.732LM(n_t)^2}{hw} \tag{4}$$

where, L is the length of the specimen, M is the mass of the specimen, n_l is the longitudinal resonance frequency, n_t is the torsional resonance frequency, h is the height of the prism cross section, and w is the width of the prism cross section.

2.2.3 Suspension Damping Loss Factor Test

Three prism specimens for each material were prepared for the damping ratio test. The setup is the same as in Fig. 1a, following ASTM C215-19 (ASTM, 2019), and the damping ratio was calculated as in Eqs. (5) and (6):

$$\xi = \frac{f_1 - f_2}{2f_0} \tag{5}$$

$$\eta = 2\xi \tag{6}$$

where ξ is the damping ratio of the specimen; f_0 is the resonance frequency of the specimen; f_1, f_2 is the frequency corresponding to an amplitude of $A_{max}/\sqrt{2}$, as shown in Fig. 2; and η is the damping loss factor. Figure 3 shows the time domain data and the frequency domain results after FFT analysis.

3 Numerical Methods

3.1 Train–Track Model

In the simulation, the load from the railway system should be defined first, and the train–track model is an efficient

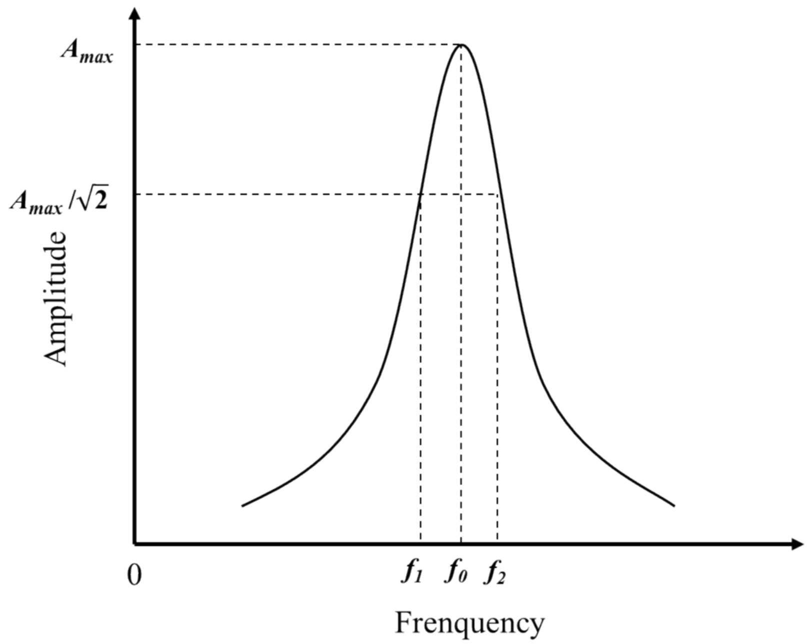

Fig. 2 Half-power bandwidth method used to estimate the damping ratio of cementitious specimens (Wu & Pyo, 2023)

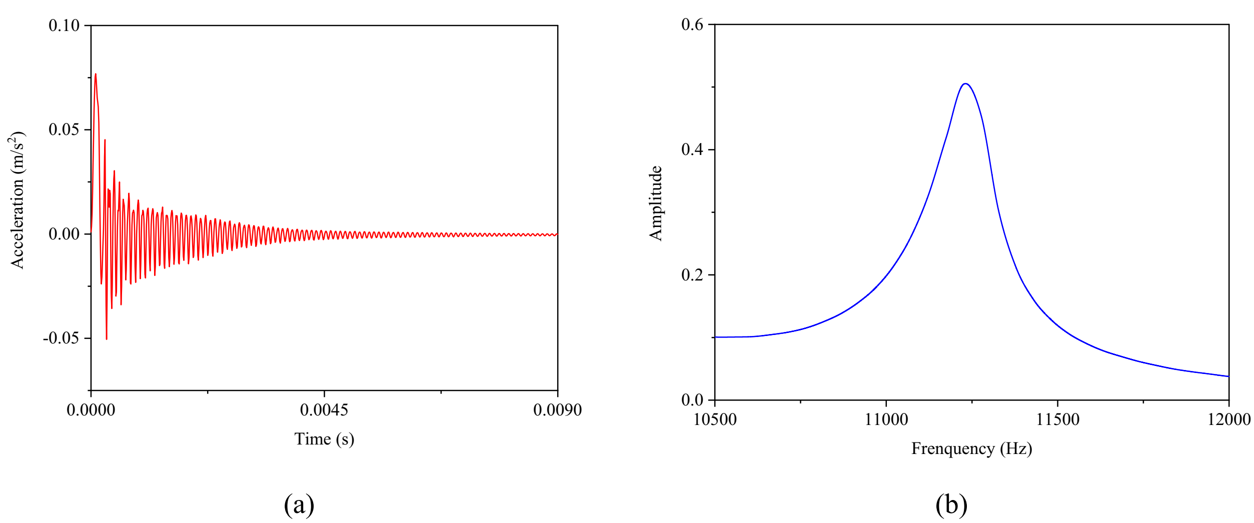

Fig. 3 **a** Time-domain signal, **b** frequency-domain results after FFT analysis

and effective way to do so because of the dynamic interaction between the train and track structure (Zhai et al., 2009, 2013). Moreover, this loading causes vibration, which can be transmitted through buildings and which generates structure-borne noise. Therefore, the vibration can be considered composed of a train model and a track model, the loadings of which were determined by Zhai et al. (Zhai et al., 2013) using their Eqs. (7) and (8), respectively:

$$\mathbf{M}_{\mathrm{r}}\ddot{\mathbf{a}}_{\mathrm{r}} + \mathbf{C}_{\mathrm{r}}\dot{\mathbf{a}}_{\mathrm{r}} + \mathbf{K}_{\mathrm{r}}\mathbf{a}_{\mathrm{r}} = \mathbf{P}_{\mathrm{r}} \tag{7}$$

where $\ddot{\mathbf{a}}_{\mathrm{r}}$, $\dot{\mathbf{a}}_{\mathrm{r}}$, and $\mathbf{a}_{\mathrm{r}}$ are the acceleration, velocity, and displacement vectors for the train model, respectively, and $\mathbf{M}_{\mathrm{r}}$, $\mathbf{C}_{\mathrm{r}}$, $\mathbf{K}_{\mathrm{r}}$, and $\mathbf{P}_{\mathrm{r}}$ are the mass matrices, damping matrices, stiffness matrices, and load vector matrices of the train model, respectively. Furthermore

$$\mathbf{M}_{\mathrm{t}}\ddot{\mathbf{a}}_{\mathrm{t}} + \mathbf{C}_{\mathrm{t}}\dot{\mathbf{a}}_{\mathrm{t}} + \mathbf{K}_{\mathrm{t}}\mathbf{a}_{\mathrm{t}} = \mathbf{P}_{\mathrm{t}} \tag{8}$$

Table 3 Parameters of the train–track model (Zou et al., 2020)

Name	Unit	Value	Name	Unit	Value
Car length	mm	19,520	Elastic modulus of sleeper	MPa	30,000
Car body mass	kg	42,600	Poisson's ratio of sleeper	–	0.2
Bogie mass	kg	2550	Sleeper density	kg/m^3	2400
Distance between two bogie centers	mm	12,600	Sleeper spacing	m	0.6
Distance between two axles of a bogie	mm	2300	Sleeper size	mm^3	$2500\times220\times160$
Suspension stiffness	kN/mm	1.5	Elastic modulus of ballast and sub-ballast	MPa	300
Wheelset mass	kg	1760	Poisson's ratio of ballast and sub-ballast	–	0.35
Elastic modulus of rail	MPa	210,000	Ballast density	kg/m^3	1800
Poisson's ratio of rail	–	0.25	Sub-ballast density	kg/m^3	2200
Rail density	kg/m^3	7850	Ballast and sub-ballast bulk damping	N·s/m	1.6×10^5
Area of rail cross section	m^2	7.745×10^{-3}	Ballast and sub-ballast shear damping	N·s/m	8×10^4
Rail pad damping	N·s/m	5×10^4	Cross section of ballast	mm^2	3300×250
Rail pad stiffness	N/m	1.0×10^8	Cross section of sub-ballast	mm^2	3300×200

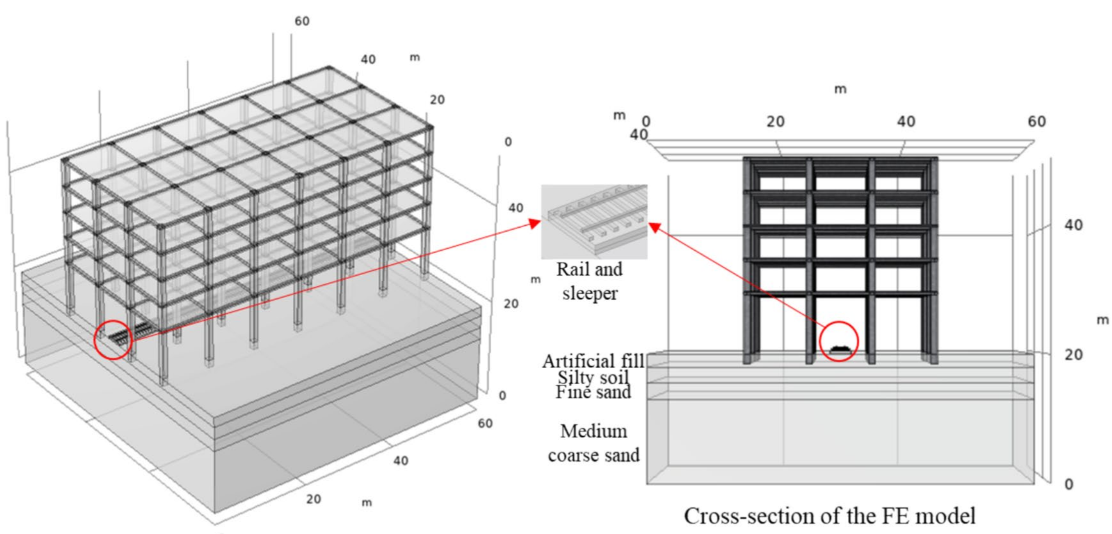

Fig. 4 FE model for verification

where $\ddot{\mathbf{a}}_t$, $\dot{\mathbf{a}}_t$, and $\mathbf{a}_t$ are the acceleration, velocity, and displacement vectors for the track model, respectively, and $\mathbf{M}_t$, $\mathbf{C}_t$, $\mathbf{K}_t$, and $\mathbf{P}_t$ are the mass matrices, damping matrices, stiffness matrices, and load vector matrices of the track model, respectively. For the simulation, the train is assumed moving along the track at a constant speed (60 km/h), so the relative displacement between cars can be neglected. The parameters for the train–track dynamic model equations are shown in Table 3.

3.2 Verification of the FE Model

After defining the railway system load, the FE model is constructed, consisting of track, soil, and buildings, as shown in Fig. 4. The soil properties and building composite parameters are shown in Tables 4 and 5, respectively. The foundation of the FE model consists of artificial fill, silty soil, fine sand, and medium coarse sand layers. The dimensions of each layer are $60\times60\times20$ m. This building structure is over the track. The bottom of each column is located 1.5 m below the ground surface. The height of the first floor is 9.5 m, and the other floors are 5.0 m. The cross-sectional dimension for each beam and column is 0.5×0.5 m^2 and 1.0×1.0 m^2. The train–track parameters are shown in Table 3.

In this study, this FE model is constructed with COMSOL (COMSOL, 2022), the results from which are verified by comparing with the field measurement method, as shown in Fig. 5. The measured results are from the studies of Zou et al. (Zou et al., 2015, 2020). The FE model also chose two locations to obtain the velocity data,

Table 4 Parameters of soil properties (Zou et al., 2020)

Soil	Thickness (mm)	Density (kg/m^3)	Elastic modulus (MPa)	Poisson's ratio	Shear wave velocity (m/s)	Pressure wave velocity (m/s)	Damping loss factor
Artificial fill*	2.0	1.98	205	0.31	198.7	387.7	0.03
Silty soil*	2.5	1.53	120	0.35	170.3	354.5	0.03
Fine sand*	2.5	1.74	220	0.23	225.4	380.6	0.03
Medium coarse sand*	13.0	1.96	280	0.25	240.2	416.0	0.03

*The dimensions of soil layers are 60 × 60 × 20 m. Artificial fill, silty soil, fine sand, medium coarse sand are soil layers, and all of them have the samedimension

Table 5 Parameters of the building composites (Zou et al., 2020)

Name	Unit	Value
Column size*	m^2	1.0 × 1.0
Beam size	m^2	0.5 × 0.5
Floor thickness	M	0.2
First floor height	M	9.5
Other floors height	M	5.0
Concrete elastic modulus	GPa	30
Concrete density	kg/m^3	2500
Concrete damping loss factor	–	0.02

*The column is 1.5 m below the ground surface. The column corresponds to the column size

which corresponds to the previous study (Zou et al., 2020, 2015). One is on the third floor, and another is on the ground 12 m away from the track centerline. It can be found that the results from the FE simulation are proximal to the field measurement results, so this FE analysis method provides another possible and accurate method for predicting train-induced vibrations. The number of elements is 742,663, and the computation of this model used 12 cores of the supercomputing system, spanning approximately 9 h.

3.3 Simplification of the FE Model

It has been proven effective in predicting vibration based on the used FE model in Sect. 3.2. This study aims to verify whether vibration-reducible materials can effectively reduce vibration and structure-borne noise on a structural level. The single solid mechanics module for vibration analysis is insufficient in this study. Therefore, the acoustic–solid interaction coupling module in COMSOL is used in this section (COMSOL, 1998, 2022). This multiphysics numerical analysis method provides a possible method for analyzing sound pressure and vibration displacement simultaneously. However, simply applying the coupling module to the FE model in Sect. 3.2 will induce more elements and degrees of freedom. To increase the computation efficiency, the building is reduced to four floors, and soil layers are shrunk to 50 × 50 × 20 m. Besides, for an accurate analysis of the acoustic–solid interaction module, it is better to add wall structures to the four sides of the building, and the walls in the train passage direction are defined as perfectly matched layers to avoid infinite sound reflection (COMSOL, 1998). If there is no barrier between indoors and outdoors, the indoor air will completely reflect the sound in the building in the acoustic–solid interaction module of the FE analysis in COMSOL, which will lead to repeated evaluations of the sound pressure level. The wall thickness is set as 20 cm, and the FE model is labeled as Model 1 and shown in Fig. 6.

Furthermore, with the same parameters, a four-floor building is located 15 m from the center line of the track in another FE model, labeled Model 2, as shown in Fig. 7.

4 Analysis Results

4.1 Results from Model 1

4.1.1 Vibration

The building in Model 1 is based on vibration-reducible construction materials, and the vibration velocity level and displacement of each floor are shown directly in Fig. 7 and Table 6. Vibration velocity level is commonly used to describe vibration level and indirectly shows the noise level (Connolly et al., 2014). In this model, the train passes through the first floor, and the vibration and sound radiate into the air directly, which cannot show the effect of construction materials on vibration reduction. Therefore, only the second-to-fourth floors are considered in this section. As shown in Fig. 8, the overall vibration velocity level of buildings with vibration-reducible materials is lower on each floor than the RF material. Especially at certain frequencies, a significant decrease in the vibration level of the building with vibration-reducible materials can be observed. For example, the vibration velocity level difference between buildings with RF materials and buildings with vibration-reducible materials can reach 12 dB at 50 Hz on the second floor, as shown in Fig. 8a. Besides, the vibration velocity levels of buildings with different materials have different variation trends, meaning not only does the damping loss factor affect the vibration response, but the other characteristics of

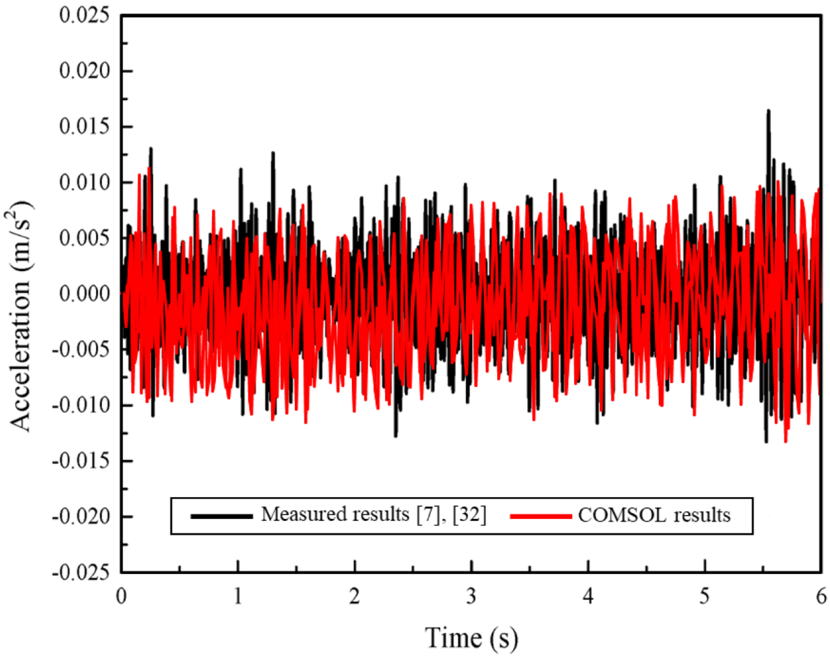

(a)

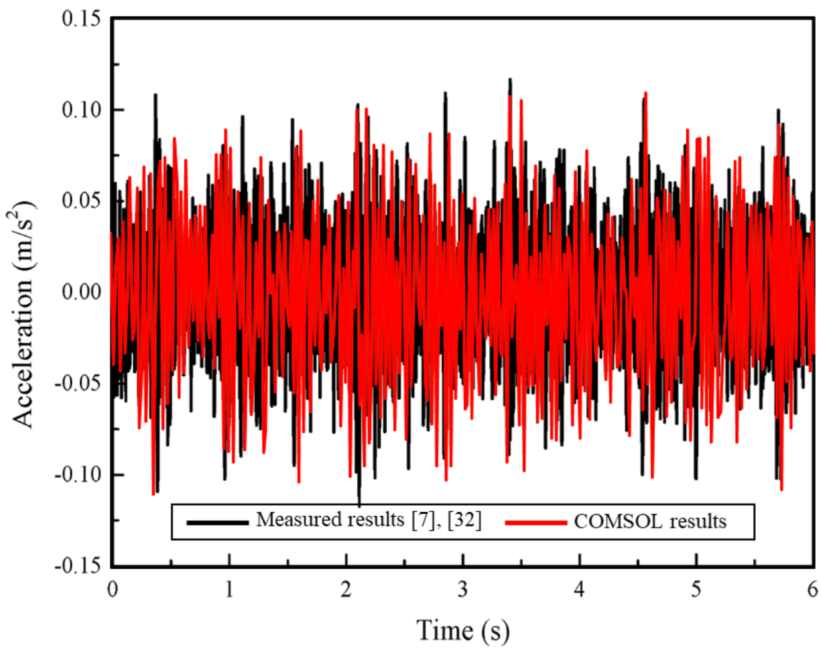

(b)

Fig. 5 Comparison of measured results and COMSOL simulation results: **a** on the 3rd floor, **b** on the ground 12 m from the track center line

cementitious materials also affect the vibration response within a building structure (Connolly et al., 2014).

Moreover, as shown in Fig. 8, the displacement and vibration velocity levels are lower on the higher floor. However, when higher than 100 Hz, the displacement and vibration velocity level of buildings with vibration-reducible materials have no significant fluctuation. Notably, the displacement of buildings with all materials decreases to around 1 μm over 100 Hz, and the results show that relatively significant displacements appear

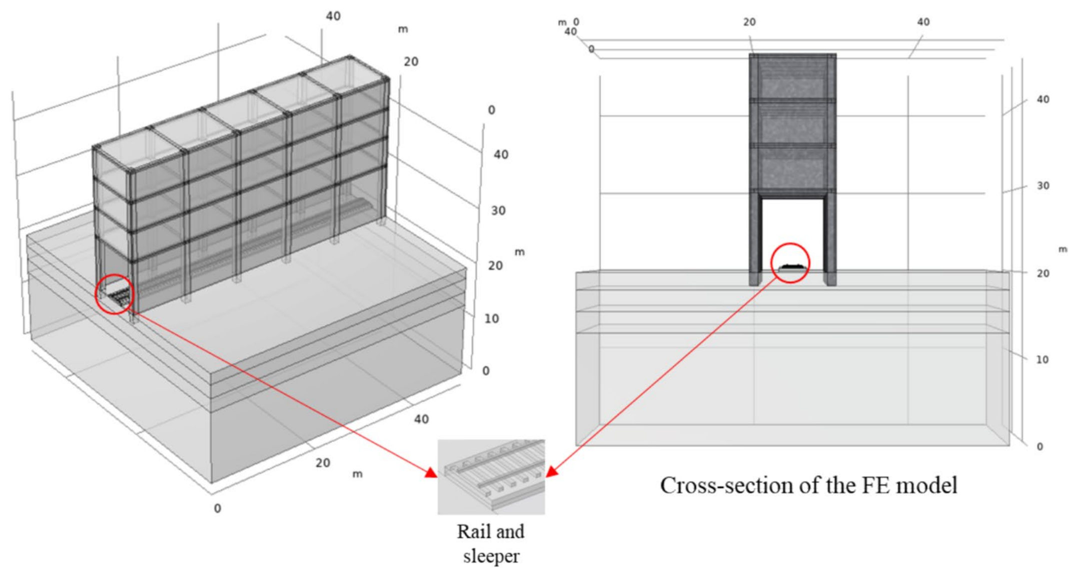

Fig. 6 Model 1: the track is located at the center of the 1st floor in the building

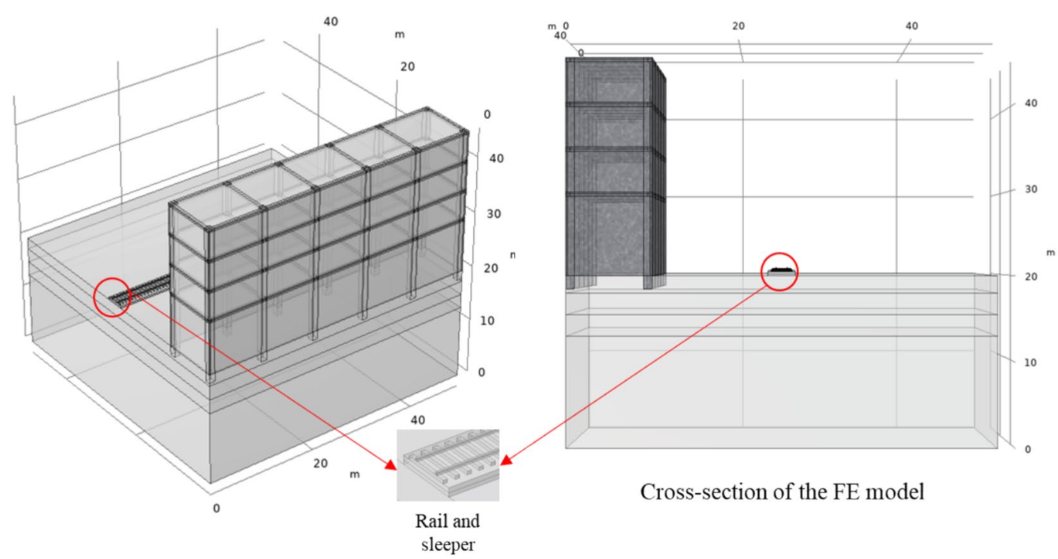

Fig. 7 Model 2: the building is located 15 m from the center line of the track

Table 6 Average vibration velocity level and displacement on each floor

Material	Velocity level at each floor (dB)			Displacement at each floor (μm)		
	Second	Third	Fourth	Second	Third	Fourth
RF	93.31	89.64	87.71	3	2.24	1.73
Material 1	92.29	87.60	85.30	2.56	1.77	1.5
Material 2	91.87	87.57	85.10	2.88	1.68	1.38
Material 3	91.08	86.53	83.96	2.48	1.81	1.33
Material 4	91.21	86.77	84.42	2.75	1.64	1.43

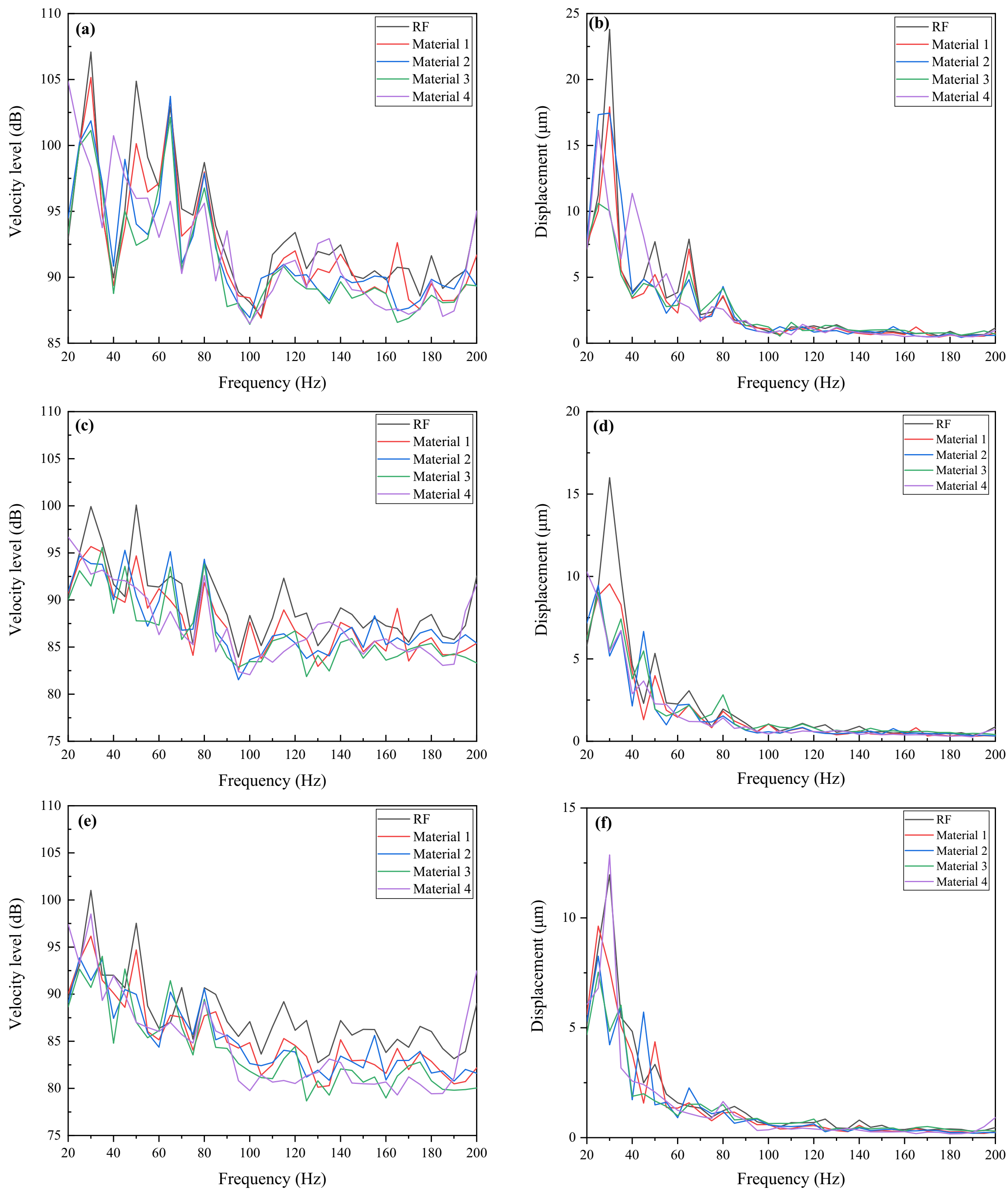

Fig. 8 **a** Vibration velocity on second floor, **b** displacement on second floor, **c** vibration velocity on third floor, **d** displacement on third floor, **e** vibration velocity on fourth floor, **f** displacement on fourth floor

from 20 to 100 Hz, corresponding to the previous study results (Zou et al., 2020).

Table 6 shows the average vibration velocity level and displacement from 20 to 200 Hz, and the average vibration of buildings with vibration-reducible materials can

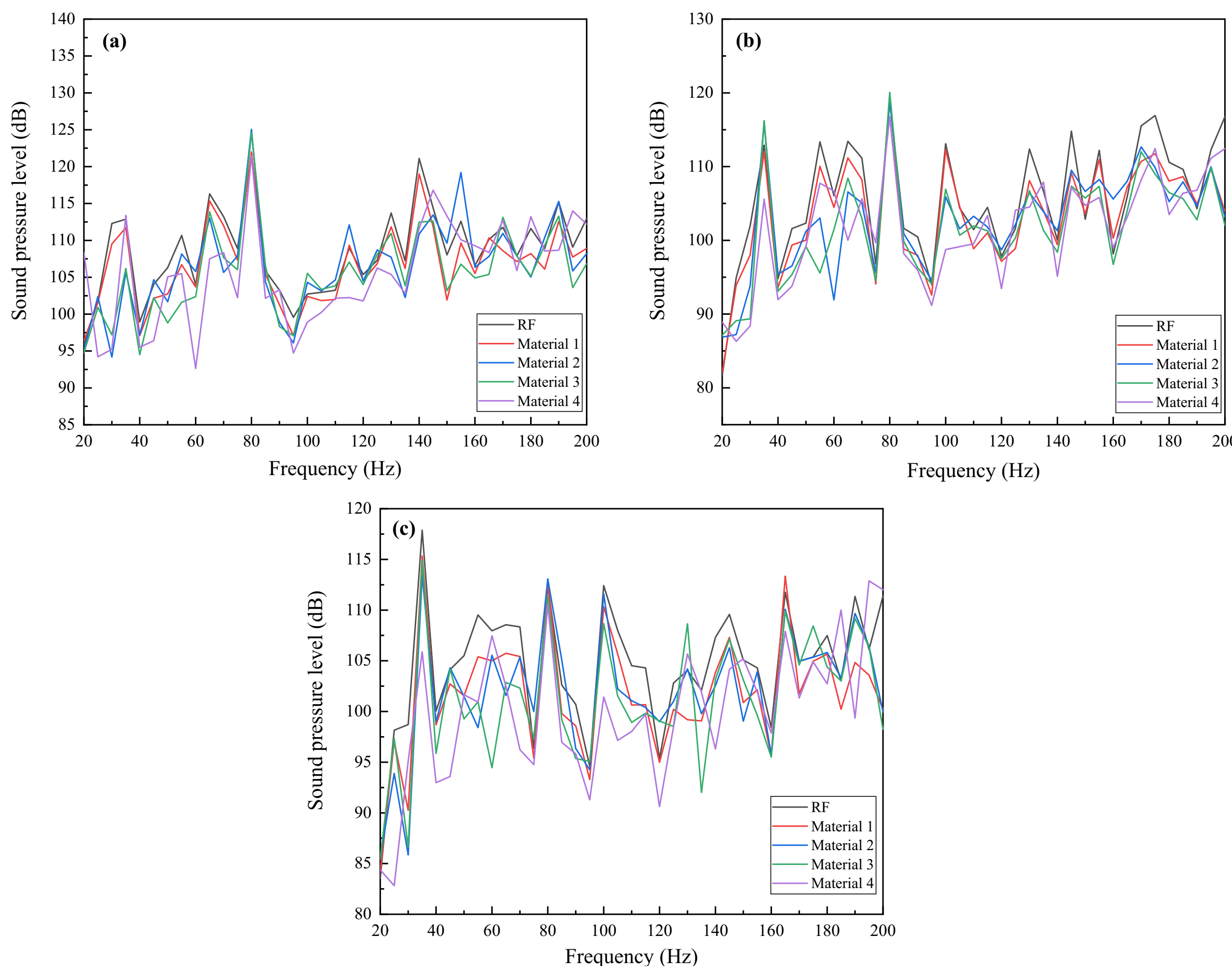

Fig. 9 Sound pressure level on: **a** second floor, **b** third floor, **c** fourth floor

be reduced by 1 dB to 3.8 dB on all floors compared to RF materials. This can be considered a significant decrease in the vibration velocity level (Sun et al., 2017). In terms of displacement, the average can decrease by up to 27% on all floors compared to the RF material. According to both results, Material 3 shows relatively better vibration reduction effectiveness among all materials, although Material 4 has a higher damping loss factor. Material 3 reduces the vibration velocity level by 7.1 dB from the second-to-fourth floors because of the higher elastic modulus and damping loss factor of Material 3, which can increase vibration energy loss and reduce structure deformation (Chi et al., 2019; Wang et al., 2017).

4.1.2 Sound Pressure Level

Figure 9 shows the sound pressure level in the building in a low-frequency range. The sound on the first floor directly radiated from the passage of the train and did not transmit through the structure. Therefore, the sound pressure level is not shown in this section. As shown in Fig. 9, the sound pressure level of buildings with vibration-reducible materials is lower than the RF material-based building from the second-to-fourth floors. Moreover, the sound pressure level results from the acoustic–solid interaction module correspond to the general measured results from a previous study (Okumura & Kuno 1991). It can be found that the maximum peak sound pressure level for all vibration-reducible material-based buildings is in the 40 to 90 Hz range. Similar to the vibration velocity level results, the variation trends of all materials differ from each other, revealing that the noise level is also affected by other mechanical properties instead of only the damping loss factor. This can be presented in detail, as shown in Table 7. The average sound pressure level on all floors decreases as the floor height increase, and the sound pressure level of vibration-reducible material-based buildings on the second-to-fourth floors can be reduced by 1.7 dB to 4.5 dB compared to the RF material. In this section, the relatively better material is Material 4, which is different from that in Sect. 4.1.1,

Table 7 Average sound pressure level and displacement at each floor

Material	Sound pressure level on each floor (dB)		
	Second	Third	Fourth
RF	108.57	105.62	104.56
Material 1	106.88	103.49	101.78
Material 2	106.60	102.91	102.04
Material 3	105.51	101.81	101.15
Material 4	105.69	101.69	100.06

as it can reduce 5.6 dB from the second-to-fourth floors, which is higher than other materials. This might be because of the lower elastic modulus compared to other materials, which causes vibration amplitude amplification in Model 1, and this corresponds to the vibration velocity level and displacement. Thus, amplified vibration can increase the energy dissipation so that less sound is transmitted (Chandra et al., 2003; Chi et al., 2019), but the reduction effect is not significant compared to other materials.

4.1.3 Structure-Borne Noise

Structure-borne noise can be calculated with the one-third octave band of the sound pressure level on the contact boundary between the air and the floor in the COMSOL acoustic module (COMSOL, 1998). Figure 10 shows results on the second-to-fourth floors, where the maximum frequency range was around 180 Hz due to the one-third octave band plot in COMSOL. It can be found that Material 1 causes higher structure-borne noise levels than other materials, between 40 and 60 Hz and at 160 Hz on the second floor, as shown in Fig. 10a. This is due to the structure-borne noise amplification on the second floor within the building, based on Material 1. Besides, this phenomenon also indicates that the transmission distance affects the vibration–reduction effect. However, on the third and fourth floors, vibration-reducible materials decrease structure-borne noise more than the RF material, as shown in Fig. 10b, c, respectively. Material 4 is a relatively better material in structure-borne noise reduction, which can be decreased by 3.7 dB on the third floor compared to the RF material. This corresponds to the sound pressure level results in Sect. 4.1.2.

Moreover, as shown in Table 8, comparing the average noise difference from the second-to-fourth floors shows that the average noise level reduction effect decays with an increase in floor height. In addition, Table 8 presents the proportion of average structure-borne noise in the average sound pressure on the second-to-fourth floors, revealing that the proportion also decreases by 1 to 2% with an increase in floor height due to the decreased vibration transmission.

4.2 Results from Model 2

4.2.1 Vibration

In Sect. 4.1, it is shown that four kinds of materials can effectively reduce vibration transmission when a train passes through the first floor of a building. However, many buildings are adjacent to railway systems, leaving them affected by the vibrations from trains passing in daily life. Similarly, the vibration transmits directly from the ground to the second floor, so this section does not include the vibration on the first floor. Figure 11 shows the vibration velocity level and displacement on the second-to-fourth floors in buildings, respectively, demonstrating that the distance between the building and the vibration resource influences the trend of vibration variations. The vibration velocity level of buildings with different materials decreases with an increase in frequency from the second-to-fourth floors. As shown in Fig. 11a, c, and e, all vibration-reducible materials can decrease the vibration velocity level, except in the 20–30 Hz frequency range, as the RF material can cause a greater loss of vibration energy at this frequency range due to its superior mechanical properties (Lopes et al., 2014; Persson et al., 2016).

Moreover, as shown in Fig. 11b, d, and f, all vibration-reducible materials can reduce the displacement on each floor compared to the RF material. However, the peak displacement of the RF material on the fourth floor was higher than that on the third floor, between 20 and 40 Hz, as the different distances between the building and the vibration resource and different materials can generate different vibration amplitude amplification regions in the horizontal direction, especially on the top floor (Sun et al., 2017). This is the reason for the higher peak displacement on the third floor with different materials.

Besides, Table 9 shows the average vibration velocity level and displacement results. It can be found that the vibration velocity level decreases with an increase in floor height. The average vibration velocity level can be reduced by 0.5 dB to 3.2 dB compared to the RF material. However, for displacement, it is revealed that the average displacement of buildings based on the RF material on the third floor is higher than that on the fourth floor, because the vibration amplitude amplification effect induces higher displacement peaks in some frequency ranges. In terms of the vibration velocity level, Material 4 is also the relatively better material in Model 2, reducing the vibration velocity by 6 dB from the second-to-fourth floors. Conversely, although Material 4 has a better damping loss factor, the displacement reduction is less

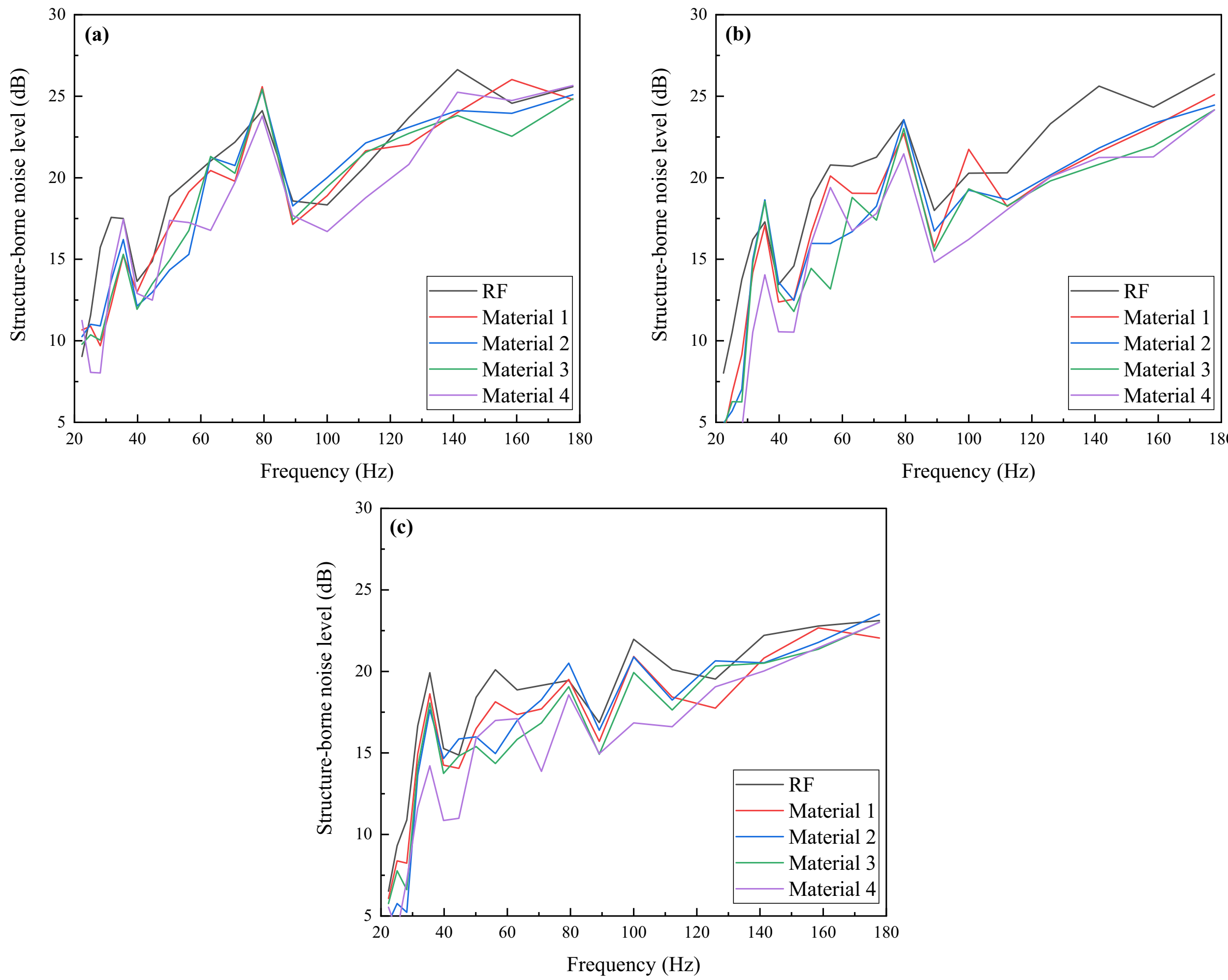

Fig. 10 Structure-borne noise on **a** second floor, **b** third floor, **c** fourth floor

Table 8 Average structure-borne noise level and the proportion of structure-borne noise in the average sound pressure on the second-to-fourth floors

Material	Structure-borne noise level on each floor (dB)			The proportion of structure-borne noise in the average sound pressure (%)		
	Second	Third	Fourth	Second	Third	Fourth
RF	19.16	18.79	17.68	17.65	17.79	16.91
Material 1	18.06	16.81	16.43	16.90	16.24	16.14
Material 2	17.94	16.43	16.11	16.83	15.97	15.79
Material 3	17.62	15.90	15.79	16.70	15.61	15.61
Material 4	17.30	15.10	14.68	16.37	14.85	14.67

than Material 3 due to the lower elastic modulus of Material 4, which causes a worse deformation resistance.

4.2.2 Sound Pressure Level

Figure 12 shows the sound pressure level results, demonstrating that the sound pressure level variation differs from that of the velocity level variation, with an increase in the distance between the building and vibration

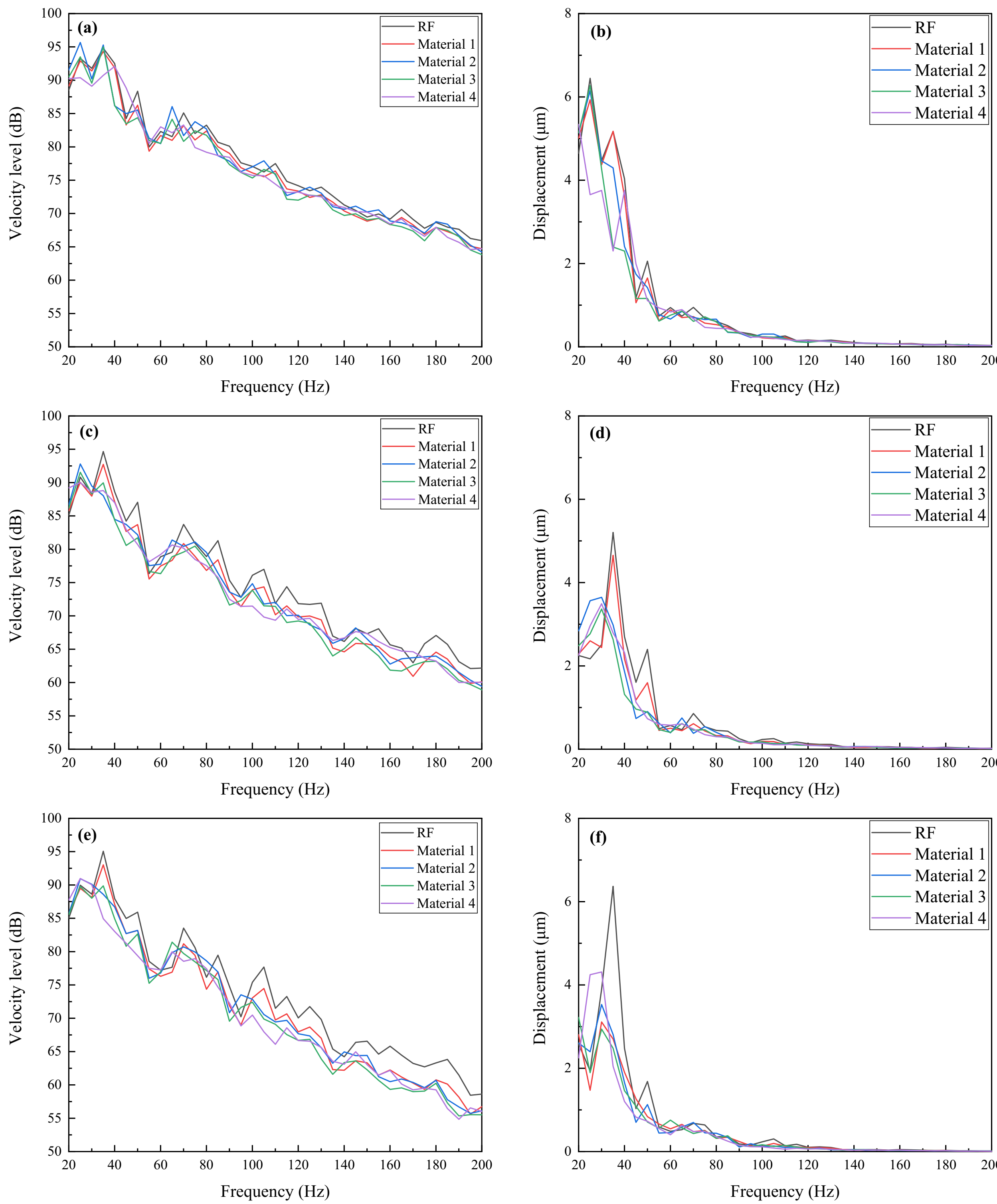

Fig. 11 **a** Vibration velocity on second floor, **b** displacement on second floor, **c** vibration velocity on third floor, **d** displacement on third floor, **e** vibration velocity on fourth floor, **f** displacement on fourth floor

Table 9 Average vibration velocity level and displacement on each floor

Material	Velocity level on each floor (dB)			Displacement on each floor (μm)		
	Second	Third	Fourth	Second	Third	Fourth
RF	77.31	74.54	73.36	0.98	0.67	0.69
Material 1	76.45	72.65	71.13	0.92	0.59	0.52
Material 2	76.81	72.90	71.11	0.89	0.58	0.53
Material 3	76.01	71.95	70.78	0.81	0.52	0.51
Material 4	76.17	72.63	70.14	0.8	0.56	0.54

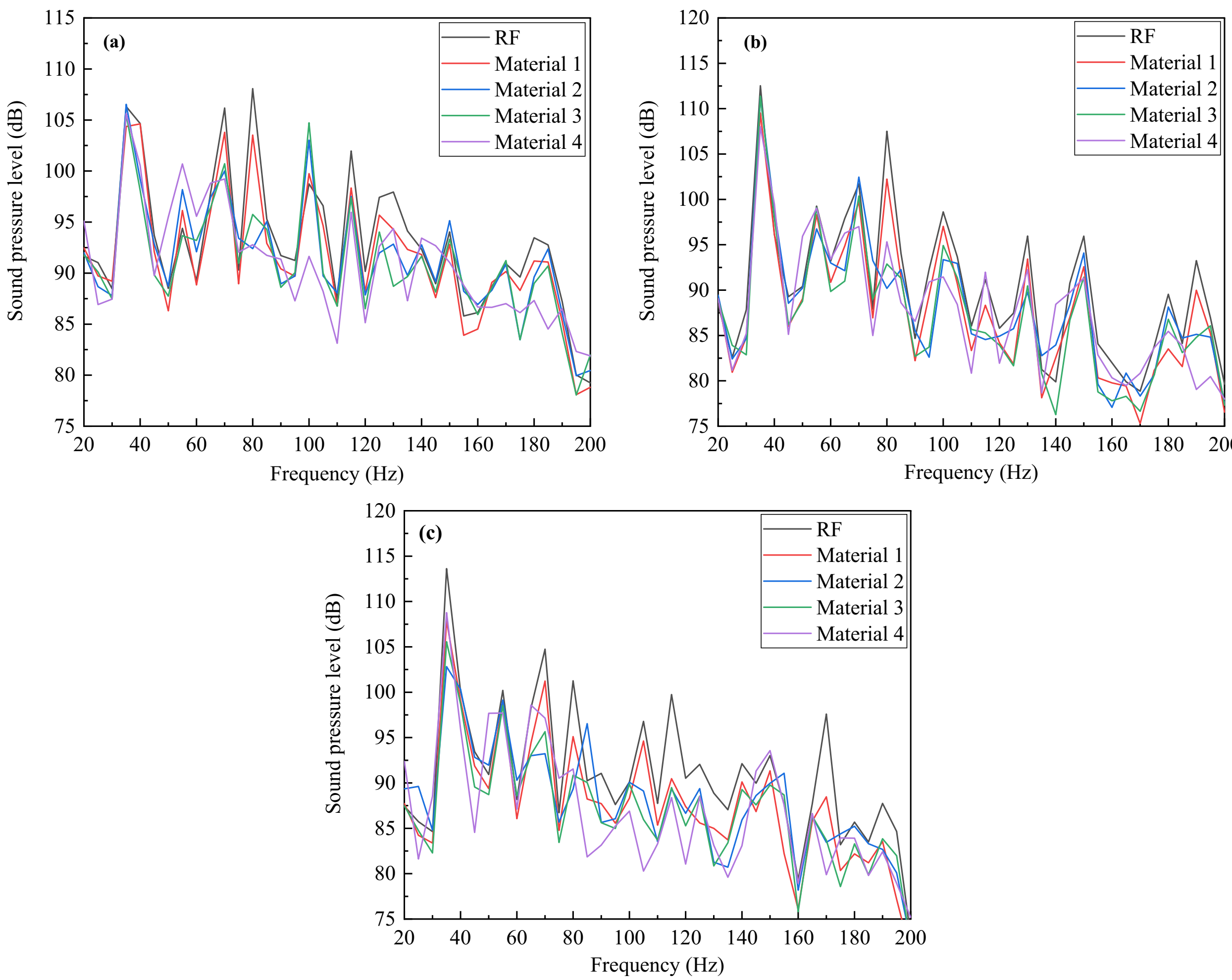

Fig. 12 Sound pressure level on **a** second floor, **b** third floor, **c** fourth floor

resources. In other words, the sound pressure level is not only related to the vibration of buildings, but also to other physical properties of construction materials that affect sound transmission, such as density, elastic modulus, and Poisson's ratio (Lopes et al., 2014). Compared to the RF material, all vibration-reducible materials decrease the sound pressure level at 80 to 140 Hz frequency ranges on each floor. For the second floor, the peak frequency appears at 80 Hz, and for the third and fourth floors, the peak frequency occurs at 40 Hz, indicating that an increased distance between buildings and vibration resources can induce different sound pressure distributions and transmissions.

Table 10 Average sound pressure level and displacement on each floor

Material	Sound pressure level on each floor (dB)		
	Second	Third	Fourth
RF	93.03	90.11	90.87
Material 1	91.67	87.67	87.64
Material 2	91.54	88.01	87.90
Material 3	90.99	86.99	86.91
Material 4	90.91	87.89	86.99

Furthermore, Table 10 gives the average sound pressure level on each floor, demonstrating that the RF material increases the sound pressure level on the fourth floor compared to the third floor. Besides, the sound pressure level decrement of other materials is very small and can be explained by the vibration amplitude amplification effect, which can cause the sound amplitude to increase due to a greater vibration energy release (Heckl et al., 1996; Sun et al., 2017). On each floor, the vibration-reducible materials can reduce sound pressure by 1.3 dB to 4.0 dB, and Material 3 can reduce 4.1 dB from the second to the fourth floors, which is higher than other materials in Model 2. Therefore, Material 3 has the best sound reduction effect among all materials in Model 2, a result that differs from that presented in Sect. 4.1.2.

4.2.3 Structure-Borne Noise

Figure 12 shows the structure-borne noise level on the second-to-fourth floors in Model 2. Different from the results of Model 1, all vibration-reducible materials can reduce the structure-borne noise on each floor, and the structure-borne noise level is over 6% lower than that in Model 1, indicating that the distance between the receiver and the sound resources affects both the structure-borne noise reduction effect and structure-borne noise level within the building. Overall, Material 3 is also a relatively better material than others, and the RF material and Material 1 show a better reduction effect on the fourth floor than the third floor due to the vibration amplitude amplification effect in Model 2, as mentioned in Sect. 4.2.1. It can also be found that the Material 3 reduction effect is not as significant as that in Model 1 due to the lower vibration level in Model 2. Besides, on the third and fourth floors, Material 4 shows a better structure-borne reduction effect after 90 Hz, which means the material with high porosity is better for the higher floors at higher frequency ranges in Model 2.

Table 11 gives the proportion of the average structure-borne noise and the average sound pressure level from the second to fourth floors for each material. All proportions are lower than those in Model, corresponding the decreased vibration velocity level and displacement. In other words, reducing vibration is an effective way to reduce structure-borne noise; thus, the overall sound pressure level can be decreased.

5 Discussion

It is shown that the distance between the building and the vibration resource affects the variations in vibration and sound. Therefore, the overall average vibration velocity level, displacement, and sound pressure of both models will be compared and discussed in detail.

5.1 Vibration

Figure 13a shows the overall average vibration velocity level of all floors of buildings with all materials in this study. It is obvious that the distance between building and vibration is one of the essential parameters that can significantly reduce the vibration velocity level by about 10 dB for all buildings. This corresponds to the previous study (Kouroussis et al., 2021). In terms of different models, Material 3 is better than other materials, as the overall average velocity level of the Material 3-based building is 3 dB lower than the RF material-based one in Model 1, and this value is 2.2 dB from Model 2. This indicates that the vibration-reducible materials contribute more to the vibration reduction in the short-distance situation.

Figure 13b shows the overall average displacement of all materials in both models. Compared to the vibration

Table 11 Average structure-borne noise level and the proportion of structure-borne in average sound pressure on the second-to-fourth floor

Material	Structure-borne noise level on each floor (dB)			The proportion of structure-borne noise and average sound pressure (%)		
	Second	Third	Fourth	Second	Third	Fourth
RF	12.90	11.89	12.36	13.87	13.19	13.61
Material 1	12.33	10.79	11.11	13.45	12.31	12.68
Material 2	12.41	11.06	10.66	13.56	12.57	12.12
Material 3	12.33	10.70	10.11	13.55	12.30	11.63
Material 4	11.88	11.17	10.58	13.01	12.71	12.16

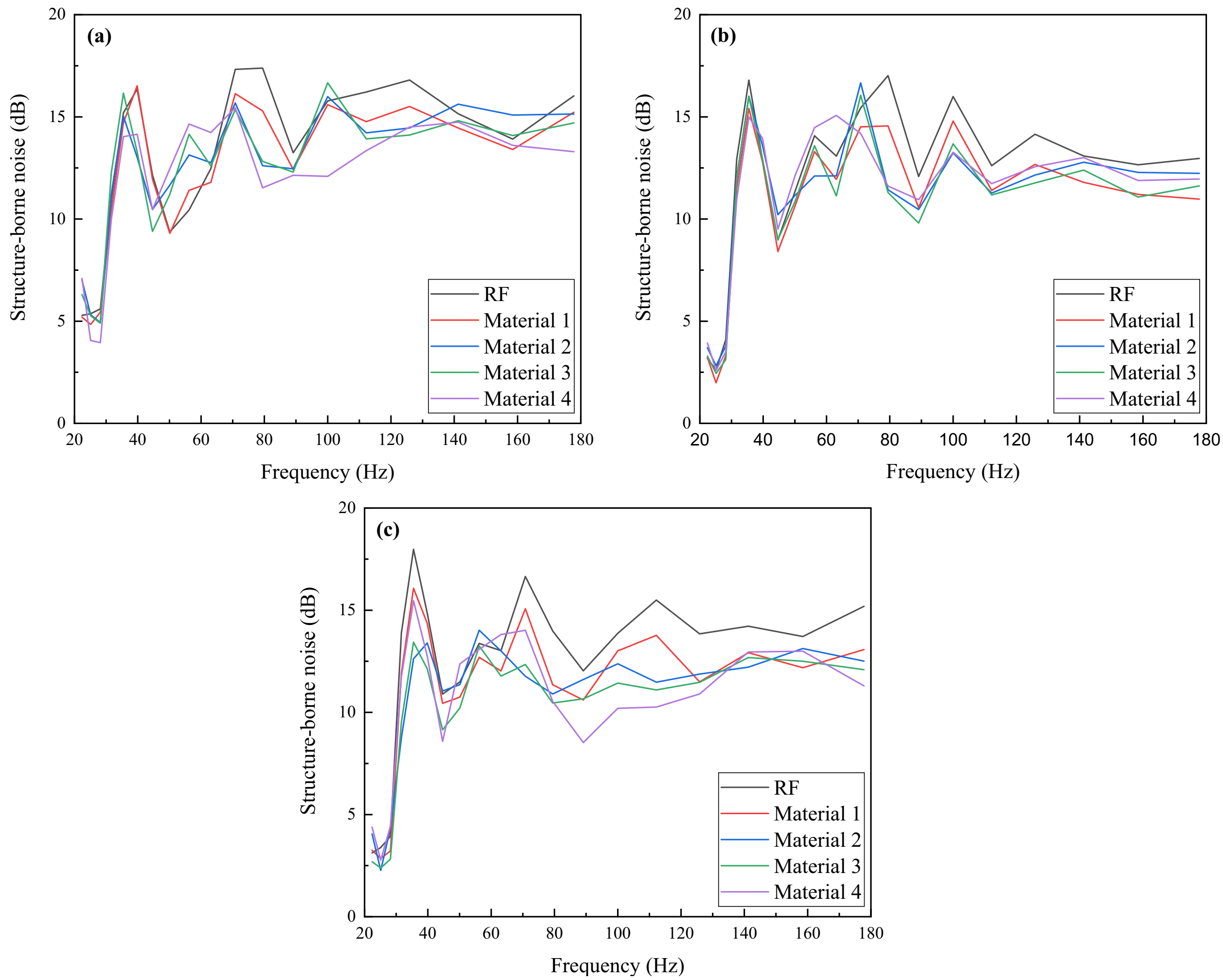

Fig. 13 Overall average **a** vibration velocity level, **b** displacement, **c** sound pressure level, and **d** structure-borne noise level for all materials in Model 1 and Model 2

velocity level decrease, the decrease in displacement can be over 65% due to the increased distance between the building and the vibration resource. Similarly, Material 3 shows the best displacement reducibility among all materials in both models. However, the decrement in the displacement of the building based on vibration-reducible materials is about 0.4 μm in Model 1 and 0.15 μm in Model 2 compared to the RF material, respectively. This reveals that the distance will affect the effectiveness of vibration-reducible materials on the vibration displacement reduction. Although the displacement results are not significant, the life service of buildings will be affected after a long-term vibration displacement (Qiu et al., 2020).

5.2 Sound Pressure Level

Figure 13c shows the overall average sound pressure level of all materials in both models, which decreases by around 11 dB with an increased distance for all materials. In Model 1, the overall average sound pressure level of the Material 4-based building is the lowest due to the relatively low elastic modulus of Material 4. In contrast, the overall sound pressure level of building Material 2 is higher than other vibration-reducible materials in Model 2. This is because the increased distance between the receiver and the vibration resource will affect the sound pressure level reduction due to the vibration amplitude amplification region. Moreover, as mentioned in Sect. 4.1.2, other mechanical properties of materials also affect the sound pressure level.

5.3 Structure-Borne Noise

As shown in Fig. 14d and Table 12, the increased distance between the receiver and sound resources decreased the overall average structure-borne noise by more than 5.4 dB. In addition, Material 4 shows the best reduction

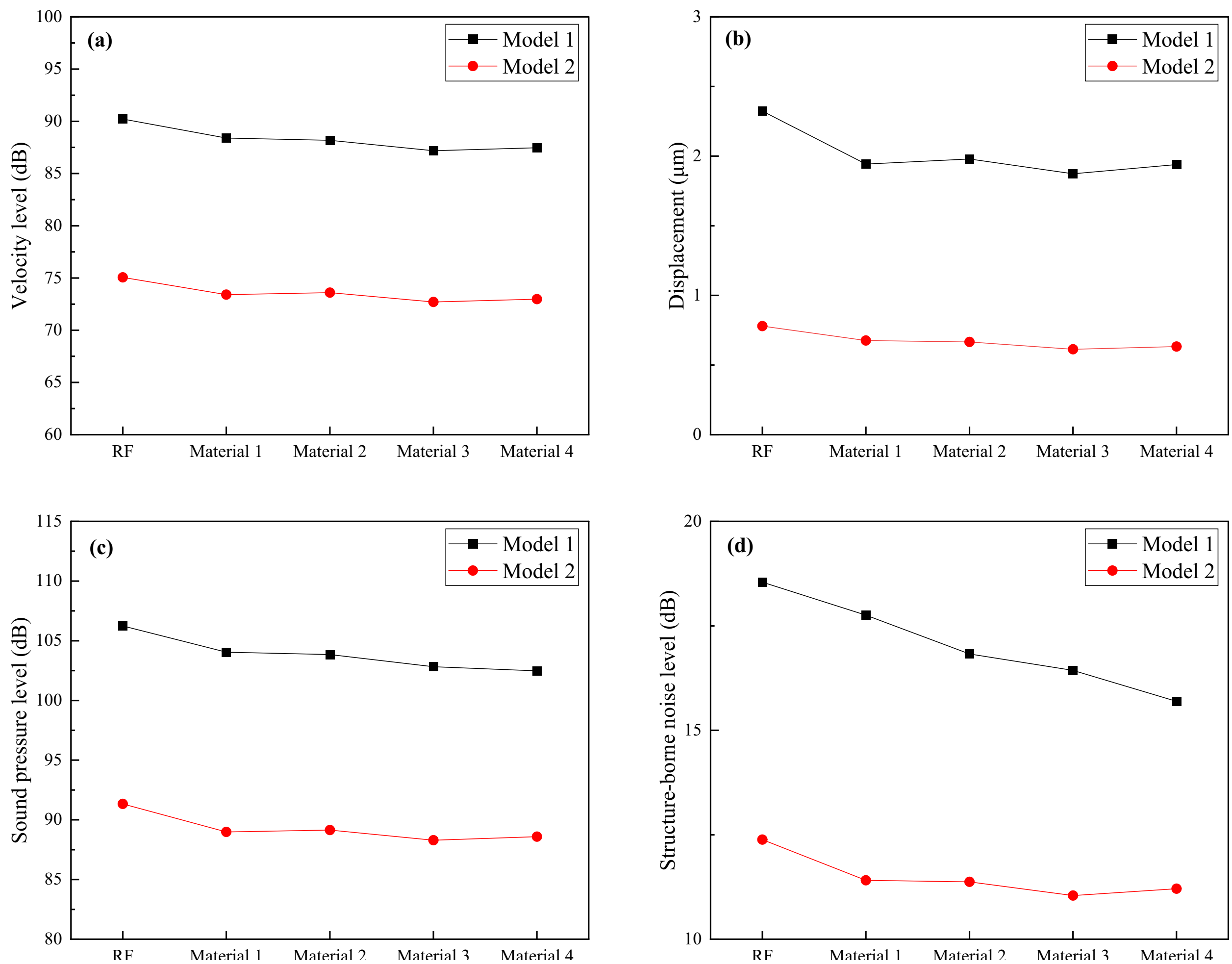

Fig. 14 Structure-borne noise on **a** second floor, **b** third floor, **c** fourth floor

Table 12 Overall average structure-borne noise level and the overall average proportion of structure-borne noise in overall average sound pressure level for all materials in Models 1 and 2

Material	Overall average structure-borne noise level of each model (dB)		The overall proportion of structure-borne noise in overall average sound pressure (%)	
	Model 1	Model 2	Model 1	Model 2
RF	18.55	12.39	17.45	13.56
Material 1	17.76	11.41	17.04	12.81
Material 2	16.83	11.38	16.20	12.75
Material 3	16.44	11.05	15.97	12.49
Material 4	15.69	11.21	15.30	12.63

effect in Model 1, able to reduce structure-borne noise by 2.9 dB compared to the RF material. In Model 2, Material 3 is the best material for structure-borne noise reduction, as it is 1.3 dB lower than the RF material. Similarly, Material 4 shows the lowest proportion of the overall average sound pressure level in Model 1, and Material 3 shows the lowest proportion out of the overall average sound pressure level in Model 2. Moreover, although Material 4 has a better damping loss factor, the overall average structure-borne noise is higher than Material 3 in Model 2, meaning the other mechanical properties of materials, such as elastic modulus and density, and even the properties of building structures also affect the structure-borne noise distribution and transmission in this study (Hudson, 1995; Ngai & Ng, 2003).

6 Parametric Study

Section 4 shows that Material 4 is better for sound pressure reductions in Model 1, while Material 3 shows a better vibration reduction and sound pressure reduction in Model 2. Further, Materials 3 and 4 are selected as reference materials in this section. Moreover, from previous sections, it can be found that not only is the damping loss factor important for vibration and sound reductions, but

Table 13 Physical properties of materials

Item	Material 3	Material 4	Material 5	Material 6	Material 7
Elastic modulus (*E*, GPa)	41.4	29.3	41.4	41.4	41.4
Poisson's ratio (*μ*)	0.26	0.21	0.21	0.21	0.26
Density (g/cm^3)	1.98	2.02	2.02	2.02	1.98
Damping loss factor (%)	1.83	1.95	1.95	2.10	2.10

Table 14 Overall average vibration velocity level and the overall average displacement in Models 1 and 2

Material	Overall average vibration velocity level of each model (dB)		Overall average displacement of each model (μm)	
	Model 1	Model 2	Model 1	Model 2
RF	90.22	75.07	2.32	0.78
Material 3	87.19	72.71	1.88	0.61
Material 4	87.74	72.98	1.94	0.63
Material 5	87.02	72.40	1.77	0.58
Material 6	86.68	71.97	1.70	0.57
Material 7	86.20	71.70	1.58	0.54

Table 15 Overall average sound pressure level and overall average structure-borne noise level in Models 1 and 2

Material	Overall average sound pressure level of each model (dB)		Overall average structure-borne noise level of each model (dB)	
	Model 1	Model 2	Model 1	Model 2
RF	106.25	91.34	18.55	12.39
Material 3	102.82	88.30	16.44	11.05
Material 4	102.48	88.60	15.69	11.21
Material 5	102.31	88.24	15.62	10.98
Material 6	102.05	88.00	15.48	10.79
Material 7	101.59	87.53	15.41	10.50

other mechanical properties are also essential for both sound and vibration reductions. Therefore, the elastic modulus and damping loss factor are the main parameters that will be investigated, including in Material 5 and Material 6, as shown in Table 13. Besides, the lower density of Material 3 may be another reason for the sound reduction and structure-borne noise reductions, so it is assumed Material 7 has the same density and elastic modulus as Material 3 and the same damping loss factor as Material 6, as shown in Table 13.

For a direct comparison, Table 14 shows the overall average vibration velocity level and displacement in both models. It can be found that Material 5 shows a lower vibration velocity level and displacement than Material 4 due to the increased elastic modulus, which can provide better deformation resistance. Furthermore, Material 6 has a higher damping loss factor than Material 5, and the vibration velocity level and displacement decreased further. Material 7 has the same damping loss factor as Material 6, and the vibration velocity can be decreased by 1 dB compared to Material 3 in both models. The displacement of Material 7 is the lowest among all; compared to the RF material, the overall average vibration velocity decreased by more than 3.5 dB in both models, which is significant in terms of the only improved mechanical properties of cementitious materials. Although Materials 6 and 7 have the same elastic modulus and damping loss factor, Material 7 shows better vibration reduction due to the lower density, which can cause a lower vibration transmission speed (Čáp et al., 2021).

Tables 14 and 15 shows the overall average sound pressure level and structure-borne noise level, where the increased elastic modulus of Material 5 only decreases the sound pressure and structure-borne noise by less than 1 dB compared to Material 4. Moreover, the increased damping loss factor and elastic modulus of Material 6 only decrease by around 0.4 dB in sound pressure and structure-borne noise. For Material 7, the increased porosity and damping loss factor can decrease sound pressure and structure-borne noise by more than 1 dB and 0.5 dB in Models 1 and 2 due to the decreased vibration velocity level, respectively. Furthermore, compared to the RF material, Material 7 decreases the sound pressure and structure-borne noise by 4.7 dB and 3.1 dB in Model 1, respectively, and in Model 2, Material 7 decreases the sound pressure and structure-borne noise by 3.8 dB and 1.8 dB, respectively.

In summary, the elastic modulus and damping loss factor are the key parameters of cementitious materials, which mainly affect the low-frequency vibration and sound reduction in building structures. The relatively low-density cementitious materials can further decrease vibration transmission.

7 Conclusions

In this study, the FE model based on the train–track model was carried out, as it has been proven valid for train-induced vibration prediction. Then, the FE model with the acoustic–solid interaction module gives a possible way to predict the train-induced vibration and sound pressure within buildings near railway systems. As well, this FE analysis method also provides a method of predicting the vibration velocity level, sound pressure level, and structure-borne noise within buildings based on different vibration-reducible cementitious materials. Moreover, the parametric study with this method investigates how the parameters of properties affect the vibration and sound levels within buildings. The key observations and findings of this research can be summarized as follows:

1) The vibration velocity level of buildings decreases with an increase in floor height. Among the four vibration-reducible materials that were used in this study, Material 3 reduced the vibration velocity level by 7.1 dB and 5.2 dB in Model 1 and Model 2 with an increased floor height, respectively. Material 3 has the best vibration reducibility due to its relatively higher elastic modulus and damping loss factor than other materials in this study.
2) The displacement within buildings also decreases with an increase in floor height, which corresponds to the vibration velocity level. All vibration-reducible materials are effective for displacement reduction, achieving displacement of over 26%. However, the displacement of the building based on the RF materials increases on the fourth floor compared to the third floor in Model 2.
3) The increased distance between the receiver and the sound resource can create a vibration amplitude amplification region. Therefore, simply changing the location of buildings cannot reduce vibration on all floors.
4) The sound pressure level has the same trend as displacement. Similarly, the sound pressure level of the RF material-based building increases on the fourth floor compared to the third floor. The vibration amplitude amplification also affects the sound pressure level. Besides, Material 4 shows relatively better sound reducibility than other materials due to the vibration amplitude amplification effect in Model 1. Therefore, the vibration and sound reduction prediction with the developed numerical method is necessary for a vibration-reducible material-based building before implementing construction.
5) The structure-borne noise decreases with an increase in floor height and an increased distance between the receiver and sound resources. Material 4 shows a better structure-borne noise reduction effect than other materials in both models, which can reduce overall structure-borne noise by 2.9 dB in Model 1. However, in Model 2, Material 3 is better, as it can reduce overall structure-borne noise by 1.3 dB. Therefore, not only does the damping loss factor affect the structure-borne noise, but the other material properties also affect structure-borne noise transmission.
6) The parametric study reveals that the elastic modulus and damping loss factor are the key factors in low-frequency vibration and sound reduction. The lower density might be slightly effective for low-frequency vibration and sound reduction due to the decreased vibration transmission speed.

In this study, it was shown that the FE model based on the acoustic–solid mechanics interaction module is an efficient way to predict the vibration and train-induced sound pressure level in a low-frequency range. To extend the present study, additional research is needed to investigate numerically the vibration behavior of the reinforced vibration-reducible material-based buildings with different structure shapes adjacent to railway systems.

Furthermore, developing the construction cementitious material with a relatively high elastic modulus, high damping loss factor, and low density is also important for future research, and the acoustic parameters of cementitious materials require further study for accurate simulation.

Moreover, to improve the accuracy of the simulation analysis, it is imperative to explore the potential for errors in the simulation model. However, due to a scarcity of available studies providing all the necessary simulation parameters, this study is constrained to presenting only one existing FE model, constituting a limitation of this research. For future research, it is necessary to find additional models to comprehensively assess the potential for the simulation model error.

Acknowledgements
This present work uses COMSOL, which is provided by the supercomputing center of Ulsan National Institute of Science and Technology (UNIST). HGM, CS, and GF were supplied by 3M, SEOKYUNG CMT (Busan, South Korea), and Merck KGaA (Darmstadt, Germany), respectively.

Author contributions
Siyu Wu: conceptualization, methodology, software, validation, formal analysis, investigation, data curation, writing—original draft, and visualization. Sukhoon Pyo: methodology, resources, writing—review and editing, supervision, project administration, and funding acquisition.

Funding
This work was supported by the National Research Foundation of Korea (NRF) grant funded by the Korea government (MSIT) (No. RS-2023-00212366).

Availability of data and materials
The data and materials are included in the manuscript.

Declarations

Ethics approval and consent to participate
Not applicable.

Consent for publication
Not applicable.

Competing interests
The authors declare no conflicts of competing interest.

Received: 21 July 2024 Accepted: 3 November 2024
Published online: 14 February 2025

References
Ahmed, L. (2018). Dynamic measurements for determining poisson's ratio of young concrete. *Nordic Concrete Research, 58*(1), 95–106. https://doi.org/10.2478/ncr-2018-0006

AmirKaynia, B. M., Madshus, C., & Zackrisson, P. (2000). Ground vibration from high-speed trains: prediction and countermeasure. *Journal of Geotechnical and Geoenvironmental Engineering, 126*(6), 531–537.

Anson, M., & Newman, K. (1966). The effect of mix proportions and method of testing on Poisson's ratio for mortars and concretes. *Magazine of Concrete Research, 18*(56), 115–130. https://doi.org/10.1680/macr.1966.18.56.115

ASTM C469-02, Standard test method for static modulus of elasticity and poisson's ratio of concrete in compression, 2002. https://doi.org/10.1520/C0469-02E01.

ASTM C215-19, Standard test method for fundamental transverse, longitudinal, and torsional resonant frequencies of concrete specimens, 2019, https://doi.org/10.1520/C0215-19.

Auersch, L. (2005). The excitation of ground vibration by rail traffic: Theory of vehicle-track-soil interaction and measurements on high-speed lines. *Journal of Sound and Vibration, 284*(1–2), 103–132. https://doi.org/10.1016/j.jsv.2004.06.017

Bolin, K., Bluhm, G., Eriksson, G., & Nilsson, M. E. (2011). Infrasound and low frequency noise from wind turbines: Exposure and health effects. *Environmental Research Letters*. https://doi.org/10.1088/1748-9326/6/3/035103

Čáp, I., Čápová, K., Smetana, M., & Borik, Š. (2021). Mechanical waves. In I. Čáp, K. Čápová, M. Smetana, & Š Borik (Eds.), *Electromagnetic and acoustic waves in bioengineering applications*. Rijeka: IntechOpen. 10.5772/intechopen.101651.

Chandra, R., Singh, S. P., & Gupta, K. (2003). A study of damping in fiber-reinforced composites. *Journal of Sound and Vibration, 262*(3), 475–496. https://doi.org/10.1016/S0022-460X(03)00107-X

L. Chi, S. Lu, & Y. Yao. (2019). Damping additives used in cement-matrix composites: A review, *Composites Part B: Engineering*, vol. 164. Elsevier Ltd, pp. 26–36. https://doi.org/10.1016/j.compositesb.2018.11.057.

K. H. Chua, K. W. Lo, & T. Balendra. (1995). Building response due to subway train traffic.

COMSOL. (1998). Acoustics Module User's Guide. [Online]. Retrieved from www.comsol.com/blogs

COMSOL. (2022). Introduction to COMSOL Multiphysics. [Online]. Retrieved from www.comsol.com/blogs

Connolly, D., Giannopoulos, A., & Forde, M. C. (2013). Numerical modelling of ground borne vibrations from high speed rail lines on embankments. *Soil Dynamics and Earthquake Engineering, 46*, 13–19. https://doi.org/10.1016/j.soildyn.2012.12.003

Connolly, D. P., Kouroussis, G., Woodward, P. K., Giannopoulos, A., Verlinden, O., & Forde, M. C. (2014). Scoping prediction of re-radiated ground-borne noise and vibration near high speed rail lines with variable soils. *Soil Dynamics and Earthquake Engineering, 66*, 78–88. https://doi.org/10.1016/j.soildyn.2014.06.021

Fiala, P., Degrande, G., & Augusztinovicz, F. (2007). Numerical modelling of ground-borne noise and vibration in buildings due to surface rail traffic. *Journal of Sound and Vibration, 301*(3–5), 718–738. https://doi.org/10.1016/j.jsv.2006.10.019

Fu, Q., & Wu, Y. (2019). Three-dimensional finite element modelling and dynamic response analysis of track-embankment-ground system subjected to high-speed train moving loads. *Geomechanics and Engineering, 19*(3), 241–254. https://doi.org/10.12989/gae.2019.19.3.241

Heckl, M., Hauck, G., & Wettschureck, R. (1996). Structure-borne sound and vibration from rail traffic. *Journal of Sound and Vibration*. https://doi.org/10.1006/jsvi.1996.0257

D. E. Hudson. (1995). Dynamics of structures: theory and applications to earthquake engineering, by Anil K. Chopra, Prentice-Hall, Englewood Cliffs, NJ, 1995. No. of pages: xxviii + 761, ISBN 0-13-855214-2, Earthquake Engineering & Structural Dynamics, 24, *8*, 1173. https://doi.org/10.1002/eqe.4290240809.

Hunt, H. E. M. (1991). Modelling of road vehicles for calculation of traffic-induced ground vibration as a random process. *Journal of Sound and Vibration, 144*, 41–51.

Hunt, H. E. M. (1996). Modelling of rail vehicles and track for calculation of ground-vibration transmission into buildings. *Journal of Sound and Vibration, 193*(1), 185–194.

Kouroussis, G., Van Parys, L., Conti, C., & Verlinden, O. (2014). Using three-dimensional finite element analysis in time domain to model railway-induced ground vibrations. *Advances in Engineering Software, 70*, 63–76. https://doi.org/10.1016/j.advengsoft.2014.01.005

Kouroussis, G., & Verlinden, O. (2013). Prediction of railway induced ground vibration through multibody and finite element modelling. *Mechanical Sciences, 4*(1), 167–183. https://doi.org/10.5194/ms-4-167-2013

Kouroussis, G., Yang Zhu, S., & Vogiatzis, K. (2021). Noise and vibration from transportation. *Journal of Zhejiang University: Science A*. https://doi.org/10.1631/jzus.A20NVT01

Li, W. W., Ji, W. M., Liu, Y., Xing, F., & Liu, Y. K. (2015). Damping property of a cement-based material containing carbon nanotube. *Journal of Nanomaterials*. https://doi.org/10.1155/2015/371404

Liang, C., Xiao, J., Wang, Y., Wang, C., & Mei, S. (2021). Relationship between internal viscous damping and stiffness of concrete material and structure. *Structural Concrete, 22*(3), 1410–1428. https://doi.org/10.1002/suco.202000628

Lopes, P., Costa, P. A., Ferraz, M., Calçada, R., & Cardoso, A. S. (2014). Numerical modeling of vibrations induced by railway traffic in tunnels: From the source to the nearby buildings. *Soil Dynamics and Earthquake Engineering, 61–62*, 269–285. https://doi.org/10.1016/j.soildyn.2014.02.013

Maclachlan, L., Ögren, M., van Kempen, E., Hussain-Alkhateeb, L., & Waye, K. P. (2018). Annoyance in response to vibrations from railways. *International Journal of Environmental Research and Public Health*. https://doi.org/10.3390/ijerph15091887

E. K. W. Ngai and C. F. Ng. (2000). Correlation of structure-borne noise and vibration along railway viaduct, In: *The 29th International Congress and Exhibition on Noise Control Engineering*, 2000.

Ngai, K. W., & Ng, C. F. (2003). Structure-borne noise and vibration of concrete box structure and rail viaduct. *Journal of Sound and Vibration, 255*(2), 281–297. https://doi.org/10.1006/jsvi.2001.4155

Y. Okumura and K. Kuno. (1991). Statistical analysis of field data of railway noise and vibration collected in an urban area.

Persson, P., Persson, K., & Sandberg, G. (2016). Numerical study on reducing building vibrations by foundation improvement. *Engineering Structures, 124*, 361–375. https://doi.org/10.1016/j.engstruct.2016.06.020

Qiu, J., Qin, Y., Feng, Z., Wang, L., & Wang, K. (2020). Safety risks and protection measures for city wall during construction and operation of Xi'an metro. *Journal of Performance of Constructed Facilities*. https://doi.org/10.1061/(asce)cf.1943-5509.0001374

Romero, A., Galvin, P., & Dominguez, J. (2012). A time domain analysis of train induced vibrations. *Earthquakes and Structures*. https://doi.org/10.12989/eas.2012.3.3_4.297

Sharma, N., Mahapatra, T. R., Panda, S. K., & Mehar, K. (2018). Evaluation of vibroacoustic responses of laminated composite sandwich structure using higher-order finite-boundary element model. *Steel and Composite Structures, 28*(5), 629–639. https://doi.org/10.12989/scs.2018.28.5.629

Sun, C., Gao, L., Hou, B., & Yizhen, W. (2017). Analysis of vibration characteristics and influence parameters of buildings adjacent to subway line. *Journal of Beijing Jiaotong University, 41*(4), 23–30.

Verbraken, H., Lombaert, G., & Degrande, G. (2011). Verification of an empirical prediction method for railway induced vibrations by means of numerical

simulations. *Journal of Sound and Vibration, 330*(8), 1692–1703. https://doi.org/10.1016/j.jsv.2010.10.026
Wang, Z., Dai, Q., & Guo, S. (2017). Laboratory performance evaluation of both flake graphite and exfoliated graphite nanoplatelet modified asphalt composites. *Construction and Building Materials, 149*, 515–524. https://doi.org/10.1016/J.CONBUILDMAT.2017.05.100
With, C., & Bodare, A. (2007). Prediction of train-induced vibrations inside buildings using transfer functions. *Soil Dynamics and Earthquake Engineering, 27*(2), 93–98. https://doi.org/10.1016/j.soildyn.2006.06.003
Wu, S., Moges, K. A., Vashistha, P., & Pyo, S. (2023). Sustainable cementitious composites with 30% porosity and a compressive strength of 30 MPa. *Journal of Materials Research and Technology, 25*, 5494–5505. https://doi.org/10.1016/j.jmrt.2023.07.036
Wu, S., Park, S., & Pyo, S. (2022). Effect of types of microparticles on vibration reducibility of cementitious composites. *Materials, 15*(14), 4821. https://doi.org/10.3390/ma15144821
Wu, S., & Pyo, S. (2023). Micromechanical modeling of damping behavior in vibration-reducible cementitious composites. *Construction and Building Materials*. https://doi.org/10.1016/j.conbuildmat.2023.131305
Zhai, W., et al. (2013). High-speed train–track–bridge dynamic interactions–Part I: Theoretical model and numerical simulation. *International Journal of Rail Transportation, 1*(1), 3–24. https://doi.org/10.1080/23248378.2013.791498
Zhai, W., Wang, K., & Cai, C. (2009). Fundamentals of vehicle-track coupled dynamics. *Vehicle System Dynamics, 47*(11), 1349–1376. https://doi.org/10.1080/00423110802621561
Zheng, L., Sharon Huo, X., & Yuan, Y. (2008). Experimental investigation on dynamic properties of rubberized concrete. *Construction and Building Materials, 22*(5), 939–947. https://doi.org/10.1016/j.conbuildmat.2007.03.005
Zhu, Q., Wang, H., & Spencer, B. F., Jr. (2023). Investigation on vibration behavior of a high-speed railway bridge based on monitoring data. *Smart Structures and Systems, 31*(6), 585–599. https://doi.org/10.12989/sss.2023.31.6.585
Zou, C., Wang, Y., & Tao, Z. (2020). Train-induced building vibration and radiated noise by considering soil properties. *Sustainability (Switzerland)*. https://doi.org/10.3390/su12030937
Zou, C., Wang, Y., Wang, P., & Guo, J. (2015). Measurement of ground and nearby building vibration and noise induced by trains in a metro depot. *Science of the Total Environment, 536*, 761–773. https://doi.org/10.1016/j.scitotenv.2015.07.123

Publisher's Note

Springer Nature remains neutral with regard to jurisdictional claims in published maps and institutional affiliations.

Siyu Wu is a research professor in Chongqing Technology and Business Institute at Chongqing Open University, Chongqing, China and former graduate student in Department of Civil, Urban, Earth, and Environmental Engineering at Ulsan National Institute of Science and Technology (UNIST), Ulsan, Korea.

Sukhoon Pyo is an Associate Professor in the Department of Civil, Urban, Earth, and Environmental Engineering at Ulsan National Institute of Science and Technology (UNIST), Ulsan, Korea.